NJC

ROYAL SOCIETY OF CHEMISTRY

COMMUNICATION

View Article Online
View Journal | View Issue



Cite this: *New J. Chem.*, 2024, **48**, 3352

Received 27th December 2023,
Accepted 28th January 2024

DOI: 10.1039/d3nj05961h

rsc.li/njc

# Synthesis of and iodine capture with $MS_x$ ($Ag_2S$, $Bi_2S_3$, $Cu_2S$)–polyacrylonitrile composites†

Brian J Riley, * Saehwa Chong and Nathan L. Canfield

**Polyacrylonitrile (PAN) composites were produced with metal sulfides ($Ag_2S$, $Bi_2S_3$, and $Cu_2S$) using dimethyl sulfoxide as the PAN dissolution medium. Static $I_{2(g)}$ loading experiments at 130 °C show values of 723, 909, and 1095 mg $g^{-1}$ for 80$Ag_2S$–PAN, 80$Bi_2S_3$–PAN, and 80$Cu_2S$–PAN, respectively.**

Chemisorption-based technologies utilizing metal or metal-sulfide ($MS_x$) composites have been demonstrated as promising options for capture of radioiodine gas [*i.e.*, $^{129}I_{2(g)}$],[1–5] which can be released from nuclear processes including reprocessing of used nuclear fuel, nuclear accidents, or the operation of molten salt reactors. The capture of $^{129}I$, a long-lived ($t_{1/2}$ = 1.57 × $10^7$ year) radioisotope, is imperative due its high environmental mobility and natural incorporation into the human thyroid gland leading to thyroid cancer.[6] Since many metals and $MS_x$ compounds demonstrated for effective iodine gas capture are inexpensive and commercially available in particle forms, several options exist for implementing such materials in off-gas capture processes where these compounds can be embedded into passive and porous scaffolds. One such option includes utilizing polyacrylonitrile (PAN) polymers as the web to hold fine particles of the active gettering material. In some cases, active chemisorbing getters have been added in the form of high specific surface area starting materials such as nanoflowers or aerogels.[1,2,4]

These PAN composites can be readily produced in the form of small (~1–3 mm diameter) oblate spheroids that can be packed into a column for flow-through experiments in either gaseous or aqueous environments.[7–9] Three of the more promising chemisorption-based getters for capturing iodine include Ag,[10,11] Bi,[12,13] and Cu[14,15] so these were included in the current work in $MS_x$ form. While Ag has proven to be likely the most effective metal for iodine gas capture, Ag disposal is controlled in the U.S. by the Environmental Protection Agency under the Resource Conservation and Recovery Act (also includes As, Ba, Cd, Cr, Pb, Hg, and Se),[16] so alternatives are needed. Calculations performed with HSC Chemistry software (v9, Outotec, Finland) to assess thermodynamic stability of $MS_x$ compounds of $Ag_2S$, $Bi_2S_3$, and $Cu_2S$ to react with $I_{2(g)}$ to form metal-iodide ($MI_x$) compounds are provided in Fig. 1 along with the Gibbs free energies of formation ($\Delta G_f^\circ$) as a function of temperature (0–200 °C). The expected compounds are AgI (from $Ag_2S$), BiOI and $BiI_3$ (from $Bi_2S_3$), and CuI (from $Cu_2S$) along with residual sulfur. In these calculations, BiOI is the most favored of the products, with the lowest $\Delta G_f^\circ$ values over this temperature range.

In this study, several $MS_x$–PAN composites were produced using a previously reported process[3,7,17,18] where $MS_x$ = $Ag_2S$ (75, 80, or 90 mass%), $Bi_2S_3$ (80 mass%), or $Cu_2S$ (80 mass%). For each batch of composite beads, the general process was the same and all were prepared separately in glass beakers. First, a mass of PAN fibers ($m_{PAN}$; ×100, 3.3 dtex, 60 mm; Dralon GmbH, Dormagen, Germany) was dissolved in dimethyl sulfoxide (DMSO; ≥99.9%, Sigma Aldrich) and the amount of $MS_x$ added ($m_{MS_x}$) was chosen to match the target mass% loadings described above (see Table S1, ESI†). Sources used for the $MS_x$

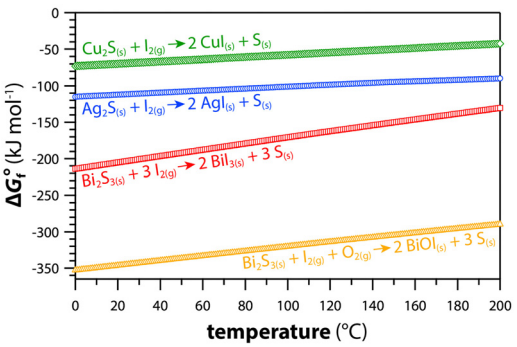


Fig. 1 Gibbs free energies of formation ($\Delta G_f^\circ$) for the $I_{2(g)}$ reactions with $Ag_2S$, $Bi_2S_3$, and $Cu_2S$ based on data from HSC Chemistry (v9).

*Pacific Northwest National Laboratory, 902 Battelle Blvd, Richland, WA 99354, USA. E-mail: brian.riley@pnnl.gov*

† Electronic supplementary information (ESI) available. See DOI: https://doi.org/10.1039/d3nj05961h



 

were from Thermo Scientific: >99.9% $Ag_2S$, 99.9% for $Bi_2S_3$, and 99.5% for $Cu_2S$. Prior to making the $Ag_2S$–PAN composites, $Ag_2S$ was ground to a fine particle size in a Diamonite mortar and pestle to further size reduce the particles. Once the PAN–DMSO–$MS_x$ mixtures were fully homogenized based on visual observations, each mixture was pipetted out of the initial mixing vessel and dropped through a 5 mL pipette tip into a stirring deionized water (DIW) bath at room temperature. After a minimum of three solution exchanges with pure DIW, the beads were removed, blotted dry, and placed into a vacuum desiccator to dry to constant mass over the course of a few weeks. Once the beads were dried, iodine uptake experiments were performed. For these experiments, $MS_x$–PAN composites and pure $MS_x$ compounds were loaded into glass vials and placed into a 1-L Savillex PFA jar along with a vial containing excess elemental iodine (99.99% Sigma Aldrich). The jar was lidded and placed into an oven at 130 ± 1 °C for 5 days at which point the iodine was removed (a dark purple iodine plume was observed), and the samples were place back in the oven for 24 h to desorb loosely bound and physisorbed iodine. Fig. S1 (ESI†) describes the general process of loading the beads with iodine and the phase distributions expected upon loading. The results of the iodine loading experiments are provided in Table 1 where the initial sample mass ($m_s$), the mass gain ($m_I$; all gain mass was attributed to iodine loading), and the iodine loading ($q_e$; mg of iodine per g of initial sorbent) are provided. The $m_I$ value was calculated as the mass difference between the sample before and after the iodine loading experiment. The extent of $MS_x$ conversion to $MI_x$ [shown in eqn (3)] of the getter metal was estimated using $q_e$ [eqn (1)] and $q_{e,max}$ [eqn (2)] based on the expected metal-iodide compound ($MI_x$, *i.e.*, AgI, $BiI_3$, and CuI) for all samples with the exception that Bi-containing iodine sorbents can also form $BiO_xI_y$ compounds (*e.g.*, BiOI, $Bi_5O_7I$).[13,19] For $q_{e,max}$, the variables $mf_{m,g}$, $MW_I$, $M_{I,MI_x}$, and $MW_m$ denote the mass fraction of metal in the $MS_x$ compound per gram of $MS_x$, molecular weight of iodine, moles of iodine in the expected $MI_x$ compound (*i.e.*, 3 for $BiI_3$), and the molecular weight of the getter metal, respectively. Based on the *C*% data, the sorbents all performed within a range of 76.7–92.5% (see Table 1).

$$q_e = 1000 \times m_I/m_s \quad (1)$$

$$q_{e,max} = 1000 \times \frac{(mf_{m,g})(MW_I)(M_{I,MI_x})}{(MW_m)} \quad (2)$$

$$C\% = 100 \times \frac{q_e}{q_{e,max}} \quad (3)$$

Table 1 Summary of iodine loading in pure $MS_x$ compounds and $MS_x$–PAN composites in terms of $q_e$ (mg $g^{-1}$). See text for descriptions of the other variables

| Sample | $m_s$ (g) | $m_I$ (g) | $q_e$ (mg $g^{-1}$) | *C* (%) |
|---|---|---|---|---|
| $Ag_2S$ | 0.1220 | 0.1156 | 948 | 92.5 |
| $Bi_2S_3$ | 0.1886 | 0.2439 | 1293 | 87.3 |
| $Cu_2S$ | 0.1269 | 0.1706 | 1344 | 84.3 |
| 75$Ag_2S$–PAN | 0.0196 | 0.0131 | 668 | 87.0 |
| 80$Ag_2S$–PAN | 0.1194 | 0.0863 | 723 | 88.2 |
| 90$Ag_2S$–PAN | 0.1585 | 0.1310 | 826 | 89.7 |
| 80$Bi_2S_3$–PAN | 0.1516 | 0.1378 | 909 | 76.7 |
| 80$Cu_2S$–PAN | 0.1546 | 0.1693 | 1095 | 85.8 |

Images of the $MS_x$–PAN composites before and after iodine loading are provided in Fig. 2. X-ray diffraction (XRD) analyses were performed on $MS_x$–PAN composites and pure $MS_x$ compounds with and without iodine using a Bruker D8 Advance XRD (Cu-$K_\alpha$). The PAN composites were crushed to flatten, and both sets of samples were loaded onto custom-made zero-background quartz holders (MTI Corporation). Phase identification and quantifications were performed using Bruker EVA and Bruker TOPAS software programs, respectively, with files from The International Centre for Diffraction Data (ICDD, PDF5+) and the Inorganic Crystal Structure Database (ICSD, v5.1.0, build 20231115-1151, release 2023.2).

The XRD data for samples before and after iodine loading are provided in Fig. 3 including both the raw data and the Rietveld refinements (calculated patterns). Comparing diffraction patterns of the $MS_x$ particles with the $MS_x$–PAN composites before iodine (Fig. 3a–c), the original $MS_x$ phase is retained within the PAN composite during production. The data for the Rietveld refinements are provided in the ESI† (see Tables S2, S3 and S4 for as-received $MS_x$ compounds, as-made $MS_x$–PAN composites, and iodine-loaded $MS_x$–PAN composites, respectively) where the $Ag_2S$ fit the monoclinic $P2_1/c$ space group (ICSD# 182916), $Bi_2S_3$ fit the orthorhombic *Pnma* space group (ICSD# 153946), and $Cu_2S$ fit the orthorhombic *Abm*2 space group (PDF# 00-09-0328, chalcocite alpha low).

The $Cu_2S$ phase with the *Abm*2 space group was not available in the ICSD so a refinement could not be run on this sample, but the PDF pattern fits nicely to the measured peak locations and intensities (see Fig. S4 and S5, ESI†). The collected patterns differed in signal-to-noise due to the small volumes analyzed, and sample displacements were observed because of the way the pellets were not entirely flattened prior to analysis in some cases. The XRD data for iodine-loaded samples are shown in Fig. 3d–f. The $Ag_2S$-containing PAN composites ($MS_x$ = 75%, 80%, and 90%) all showed mixtures of β-AgI (hexagonal $P6_3mc$ space group, ICSD# 15589) and γ-AgI (cubic $F\bar{4}3m$ space group, ICSD# 52361) with the γ-AgI phase being the dominant phase (≥70.8%; see Fig. S6, ESI†). The 80%$Bi_2S_3$–PAN+I composite was pure $BiI_3$ (trigonal $R\bar{3}$ space group, ICSD# 36182) and the 80%$Cu_2S$–PAN+I composite was pure CuI (cubic $F\bar{4}3m$ space group, ICSD# 163427). Based on the thermodynamic calculations provided in Fig. 1, the preferred compound for Bi-based sorbents based solely on $\Delta G_f^\circ$ values is BiOI over $BiI_3$, but that is not what was observed in the results from the $Bi_2S_3$ compounds in this study. While AgI and CuI are chemically stable compounds and good long-term disposal options for radioiodine, it is likely that $BiI_3$ is inferior to BiOI or other Bi-oxyiodides (*i.e.*, $Bi_5O_7I$) for long-term disposal.[12] Scanning electron microscopy (SEM) and energy dispersive X-ray spectroscopy (EDS) were conducted with a JSM-7001f field emission gun scope (JEOL USA, Inc.) and dual xFlash 6|60 (Bruker AXS Inc.) detectors, respectively. SEM micrographs and EDS dot maps are provided in Fig. 4 for the 75$Ag_2S$–PAN+I (Fig. 4a–d), 90$Ag_2S$–PAN+I

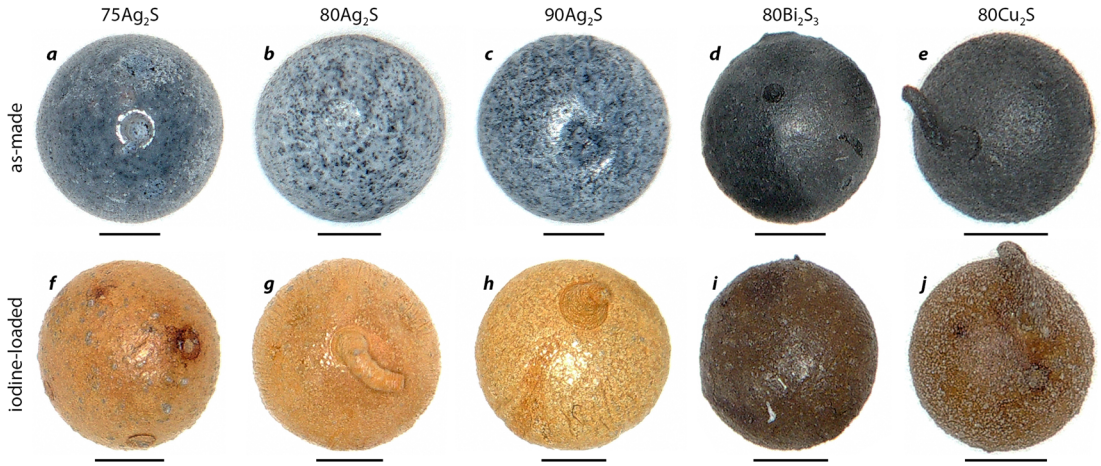


Fig. 2 Optical collage of the $MS_x$–PAN composites including (a)–(e) before and (f)–(j) after iodine loading showing (a) and (f) $75Ag_2S$–PAN, (b) and (g) $80Ag_2S$–PAN, (c) and (h) $90Ag_2S$–PAN, (d) and (i) $80Bi_2S_3$–PAN, and (e) and (j) $80Cu_2S$–PAN. The bars below each image represent 1 mm. Residual tails, which are artifacts from the bead production process, can be seen for some of the beads.

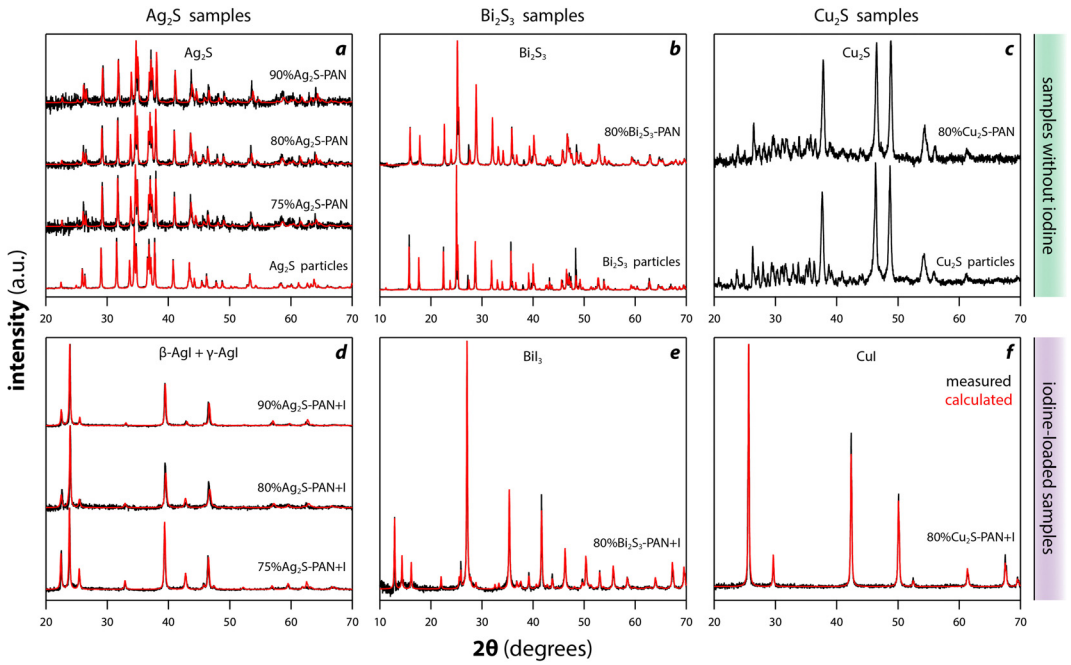


Fig. 3 Summary of XRD Rietveld refinements showing (a)–(c) before iodine loading and (d)–(f) after iodine loading for (a) and (d) $Ag_2S$-containing samples, (b) and (e) $Bi_2S_3$-containing samples, and (c) and (f) $Cu_2S$-containing samples. Measured data is provided in black and the calculated patterns from Rietveld refinements are provided in red. All spectra are shown as background subtracted. Phases identified are listed in each figure separately (see text for crystallographic information).

(Fig. 4e–h), $80Bi_2S_3$–PAN+I (Fig. 4i–l), and $80Cu_2S$–PAN+I (Fig. 4m–p) samples; additional details, micrographs, and dot maps are provided in the ESI† (see Fig. S7–S10). The calculations in Fig. 1 along with the accompanying equations also suggest residual sulfur should be present in these samples after iodine loading and this was confirmed with the sulfur dot maps shown in Fig. 4d, h, l, and p, but not seen in the XRD data. The presence of reduced forms of sulfur in iodine sorbents can also aide in preventing the production of unwanted metal compounds in the presence of oxidizing atmospheres expected in the off-gas stream of a reprocessing facility (*e.g.*, $NO_x$) as the sulfur can preferentially convert to oxides (*e.g.*, $SO_4^{2-}$) under these conditions over metal-oxide formation (of the getter) leading to a longer sorbent shelf life.[20] The PAN process allows for a method of holding these bulk sorbents in place within a passive porous network through encapsulation (like a fly in a spider web).[1] The micrographs for the $Ag_2S$ samples showed larger-sized $MS_x$ particulates in the PAN composites than the

 

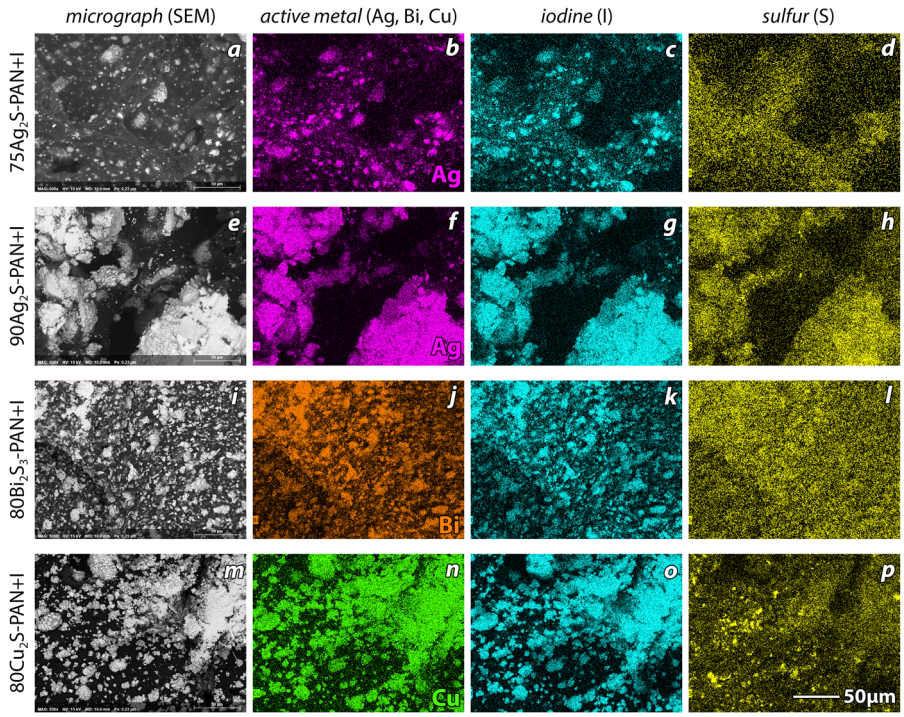


Fig. 4 SEM and EDS data for (a)–(d) $75Ag_2S$–PAN+I, (e)–(h) $90Ag_2S$–PAN+I, (i)–(l) $80Bi_2S_3$–PAN+I, and (m)–(p) $80Cu_2S$–PAN+I. All data were collected at the same 500× magnification. Darker regions in the dot maps indicate regions with low topography that were shadowed from the EDS detector.

$Bi_2S_3$ and $Cu_2S$ samples and this is attributed to the fact that the $Ag_2S$ starting material was ground by hand and the other $MS_x$ compounds were obtained commercially in finer particle sizes. The even distribution of the $MS_x$ materials within these porous polymer scaffolds and the pore structure of the PAN composite hosts should correlate to the capture efficiency for each of these sorbents, especially in conditions where the iodine concentrations are low. Recent work[21] studying iodine reactions with 0.5-mm diameter metal wires has shown that metal–iodine reactions can proceed even when the active getter is not porous. In that study,[21] the Ag wire completely reacted to form AgI while other metals (*e.g.*, Cu) did not fully react and showed a core–shell structure. This is likely due to how diffusion of iodine into bulk materials can differ substantially. This also means that highly porous sorbents might not be required in some cases to adequately capture iodine vapors.

## Summary and conclusions

In summary, PAN composites were produced using $Ag_2S$ (75, 80, 90 mass%), $Bi_2S_3$ (80 mass%), and $Cu_2S$ (80 mass%) that showed high $I_{2(g)}$ capture affinities at 130 ± 1 °C with $q_e$ values ranging from 668 mg $g^{-1}$ ($75Ag_2S$–PAN) to 1095 mg $g^{-1}$ ($80Cu_2S$–PAN) with high conversion percentages. Synthesizing these composite beads with consistent sizes and shapes is quick and easily reproducible. These benefits combined with the radiation stability of PAN[18] and high loading capacities for these materials make them promising candidates to replace commonly implemented off-gas sorbents like zeolites. Utilizing $MS_x$ compounds with higher specific surface areas (*e.g.*, nanoflowers, chalcogels)[1,2,4,22] can be implemented to achieve even better results in low-flow environments with low iodine concentrations where more active gettering sites are required.

## Author contributions

BJR – conceptualization, funding acquisition, data curation, investigation, visualization, methodology, writing – original draft, writing – review and editing. SC – data curation, investigating, methodology, writing – original draft. NC – data curation, investigating, methodology.

## Conflicts of interest

There are no conflicts to declare.

## Acknowledgements

This work was supported under an internally funded (through PNNL) Laboratory-Directed Research and Development project. Pacific Northwest National Laboratory (PNNL) is operated by Battelle Memorial Institute for the DOE under contract DE-AC05-76RL01830.

## Notes and references

1 Q. Yu, X. Jiang, Z. Cheng, Y. Liao, Q. Pu and M. Duan, *New J. Chem.*, 2020, **44**, 16759–16768.

2 Q. Yu, X. Jiang and M. Duan, *Soc. Sci. Res. Net.*, 2021, DOI: 10.2139/ssrn.3978461.
3 S. Chong, B. J. Riley, R. M. Asmussen, A. Fujii Yamagata, J. Marcial, S. Lee and C. A. Burns, *ACS Appl. Polym. Mater.*, 2022, **4**, 9040–9051.
4 B. J. Riley, D. A. Pierce, J. Chun, J. Matyáš, W. C. Lepry, T. Garn, J. Law and M. G. Kanatzidis, *Environ. Sci. Technol.*, 2014, **48**, 5832–5839.
5 B. J. Riley and S. Chong, Iodine Capture and Encapsulation, *US Pat. Appl.*, 63/596781, 2023.
6 L. B. Zablotska, E. Ron, A. V. Rozhko, M. Hatch, O. N. Polyanskaya, A. V. Brenner, J. Lubin, G. N. Romanov, R. J. McConnell, P. O'Kane, V. V. Evseenko, V. V. Drozdovitch, N. Luckyanov, V. F. Minenko, A. Bouville and V. B. Masyakin, *Br. J. Cancer*, 2011, **104**, 181–187.
7 B. J. Riley and T. Garn, in *Advances in Materials Science Research*, ed. M. Wythers, Nova Science Publishers, 2019, vol. 35, pp. 119–147.
8 F. Šebesta and V. Štefula, *J. Radioanal. Nucl. Chem.*, 1990, **140**, 15–21.
9 K. N. Brewer, T. A. Todd, D. J. Wood and P. A. Tullock, *Czech. J. Phys.*, 1999, **49**, 959–964.
10 B. J. Riley, S. Chong, J. Marcial, N. Lahiri, M. K. Bera, S. Lee, T. Wu, K. Kruska and J. Matyáš, *ACS Appl. Nano Mater.*, 2022, **5**, 9478–9494.
11 B. J. Riley, J. D. Vienna, D. M. Strachan, J. S. McCloy and J. L. Jerden Jr, *J. Nucl. Mater.*, 2016, **470**, 307–326.
12 A. Tesfay Reda, M. Pan, D. Zhang and X. Xu, *J. Environ. Chem. Eng.*, 2021, **9**, 105279.
13 Y. Hao, Z. Tian, C. Liu and C. Xiao, *Front. Chem.*, 2023, **11**, 1122484.
14 M. M. Metalidi, V. I. Beznosyuk, N. N. Kalinin, A. B. Kolyadin and Y. S. Fedorov, *Radiochemistry*, 2009, **51**, 409–411.
15 E. R. Vance, C. Grant, I. Karatchevtseva, Z. Aly, A. Stopic, J. Harrison, G. Thorogood, H. Wong and D. J. Gregg, *J. Nucl. Mater.*, 2018, **505**, 143–148.
16 40 CFR 261, Identification and listing of hazardous waste, Environmental Protection Agency, Washington, D.C.
17 B. J. Riley, S. Chong, R. M. Asmussen, A. Bourchy and M. H. Engelhard, *ACS Appl. Polym. Mater.*, 2021, **3**, 3344–3353.
18 B. J. Riley, S. Chong, W. Kuang, T. Varga, A. S. Helal, M. Galanek, J. Li, Z. J. Nelson and P. K. Thallapally, *ACS Appl. Mater. Interfaces*, 2020, **12**, 45342–45350.
19 J. H. Yang, Y.-J. Cho, J. M. Shin and M.-S. Yim, *J. Nucl. Mater.*, 2015, **465**, 556–564.
20 J. Matyáš, E. S. Ilton and L. Kovařík, *RSC Adv.*, 2018, **8**, 31843–31852.
21 B. J. Riley, S. Chong and C. L. Beck, *Ind. Eng. Chem. Res.*, 2021, **60**, 17162–17173.
22 K. S. Subrahmanyam, D. Sarma, C. D. Malliakas, K. Polychronopoulou, B. J. Riley, D. A. Pierce, J. Chun and M. G. Kanatzidis, *Chem. Mater.*, 2015, **27**, 2619–2626.

 